A STUDY OF HEAT TRANSFER IN POWER LAW NANOFLUID

by

Rahmat ELLAHI[a,b*], Mohsin HASSAN[c], and Ahmad ZEESHAN[a]

[a] Department of Mathematics and Statistics, FBAS, IIUI, Islamabad, Pakistan
[b] Department of Mechanical Engineering, University of California Riverside, Riverside, Cal., USA
[c] Department of Mathematics, Faculty of Sciences, HITEC University, Taxila Cantt, Pakistan

Original scientific paper
DOI: 10.2298/TSCI150524129E

The purpose of this paper is to study the effects of nanoparticles on mixed convection flow of power law fluid. The shear thinning fluid is considered as base fluid. The nanoparticles of copper for nanofluid are taken into account. To analysis the flow and temperature behavior, various mass concentrations of polyvinyl alcohol in water, different sizes and concentrations of nanoparticles are used. The effects of nanoparticle concentrations on shear stress, heat flux, and thermal resistance are also presented.

Key words: *mixed convection, power law model, nanofluid, shears stress, heat flux, thermal resistance*

Introduction

The heat transfer by mean of fluid flow is encountered in numerous applications such as heat exchangers, cooling systems, electronic equipment, *etc.* Most of the Newtonian and non-Newtonian fluids such as water, oil, ethylene glycol mixture, molten plastics, polymers, glues, ink, pulps, foodstuffs, and slurries are too much used in various manufacturing, industrial and engineering applications [1, 2]. To achieve the desired requirement in industry, the thermal performance of heat transfer in the conventional fluids is not appropriate because of its lower thermal conductivity. Numerous researchers have been investigating better techniques to enhance the thermal performance of heat transfer fluids. One of the methods used is to add nanosized particles of high thermal conductive materials like carbon, metals, and metal oxides into the heat transfer fluid to increase the overall thermal conductivity of the fluid [3, 5]. As a result of thermal conductivity the base fluid is dramatically enhanced in the presence of nanoparticles that is why the thermal conductivity of nanofluids has attracted the most widely attention of scientists due to its essential heat transfer properties. Sajadi *et al.* [6] reported the experimental study to improve the thermal performance of Newtonian fluid water by ZnO particles. The results indicated that heat transfer coefficient increases by 11% and 18% with increasing the volume fractions of nanoparticles to 1% and 2%, respectively. It is overall thermal performance of nanofluid which is higher than that of pure water up to 16% for 2% volume concentration of nanoparticles. Another experimentally study examined the forced convective heat transfer in non-Newtonian nanofluids through a uniformly heated circular tube under turbulent flow conditions [7]. It is observed that the local and average heat transfer coefficients of nanofluid are larger than that of the base fluid. Heat transfer enhance-

* Corresponding author emails: rellahi@engr.ucr.edu, rahmatellahi@yahoo.com

ment of nanofluids increases with an increase in nanoparticle concentration. Nadeem *et al.* [8] have studied the non-Newtonian power-law nanofluids past a linearly stretching sheet. In this study the nanoparticle concentration distribution is illustrated by Brownian motion parameter. The obtained results demonstrate that the Brownian motion of nanoparticles achieves thermal conductivity enhancement and as a result temperature distribution enhances strongly. They conclude that enhanced migration of suspended nanoparticles via the mechanisms of thermophoresis increases energy exchange rates in the fluid. Nevertheless, addition of nanoparticle improves the thermal properties even in Newtonian and Non-Newtonian base fluid [7-12].

In this paper, the shear thinning polymer solution fluid under the influence of nanoparticle on it over stretching sheet is investigated. The study of mass flow and heat transfer over a stretching sheet may find its applications in polymer technology related to the stretching of plastic sheets. Also, many metallurgical processes involve the cooling of continuous strips or filaments by drawing them through a quiescent fluid and while drawing these strips are sometimes stretched. For shear thinning fluid, power law model and mathematical model reduced into non-linearity. Due to intrinsic non-linearity of the governing equations, analytical solutions are very rare. To deal with this difficulty numerous analytical and semi analytical methods have been established. The *optical homotopy analysis method* is one of most effective technique among them to handle this obstacle. The solutions of non-linear resulting equations are carried out by using optimal homotopy analysis method [13, 14]. The behaviors of particle volume friction, particle size and concentration of polymer on the velocity, temperature, shear stress, and heat flux are analyzed through graphs.

Mathematical formulation

Consider the steady-state, incompressible, mixed convection boundary layer flow of power-law fluid over a stretching sheet. The positive x-axis is assumed along the direction of the flow and y-axis measured normal to the sheet. The flow phenomena generated as a result of linear stretching of sheet as shown in fig. 1, and shear thickening fluids and defined:

$$\tau = K\dot{\gamma}^n \tag{1}$$

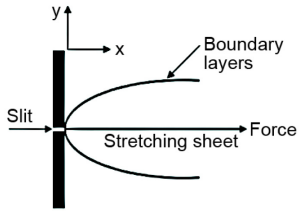

Figure 1. Geometry of the problem

where K is the consistency coefficient and n – the flow behavior index. For a special case of a Newtonian fluid ($n = 1$), when the magnitude of $n < 1$ the fluid is shear-thinning and when $n > 1$ the fluid is shear-thickening in nature. Here we consider the shear-thinning polymer solution of different consideration of polyvinyl alcohol in water. For, the nanofluid, polymer solution is used as base fluid with nanoparticle of copper. Under the Boussinesq approximation, the governing equations in component form for power law model can be written:

$$\frac{\partial u}{\partial x} + \frac{\partial v}{\partial y} = 0 \tag{2}$$

$$\rho_{\mathrm{nf}}\left(u\frac{\partial u}{\partial x} + v\frac{\partial u}{\partial y}\right) = \frac{\partial}{\partial y}\left(\mu_{\mathrm{nf}}\frac{\partial u}{\partial y}\right) + (\rho\beta)_{\mathrm{nf}}\, g(T - T_\infty) \tag{3}$$

$$\left(u\frac{\partial T}{\partial x} + v\frac{\partial T}{\partial y}\right) = \alpha_{\mathrm{nf}}\frac{\partial^2 T}{\partial y^2} \tag{4}$$

subject to boundary condition are:

$$\left.\begin{aligned} &u(x,0)=u(x)=U=ax, \quad v(x,0)=0,\\ &T(x,0)=T_\infty+A\left(\frac{x}{l}\right)\\ &u(x,\infty)=0, \quad T(x,\infty)=T_\infty \end{aligned}\right\} \tag{5}$$

In the equations, u and v are the velocity components in the x-axis and y-axis directions, respectively. In eqs. (6)-(8), the effective density, ρ_{nf}, heat capacitance, $(C_p)_{\mathrm{nf}}$, and thermal expansion coefficient, β_{nf}, of the nanofluid are defined:

$$\rho_{\mathrm{nf}}=(1-\phi)\rho_f+\phi\rho_{\mathrm{s}} \tag{6}$$

$$(\rho C_p)_{\mathrm{nf}}=(1-\phi)(\rho C_p)_{\mathrm{f}}+\phi(\rho C_p)_{\mathrm{s}} \tag{7}$$

$$(\rho\beta)_{\mathrm{nf}}=(1-\phi)(\rho\beta)_f+\phi(\rho\beta)_{\mathrm{s}} \tag{8}$$

In order to include the effect of the liquid layer, nanoparticle-in-liquid suspension with nanosize spherical particles of radius, R_{p} is used. The solid-like layer of thickness, h_{layer}, around the particles is assumed to be more ordered than that of the bulk liquid whereas the thermal conductivity, k_{layer}, of ordered layer is higher than that of the bulk liquid. We also assumed that the nanolayer around each particle could be combined with the particle to form an equivalent particle and that the particle volume concentration is so low and a result there is no overlap of those equivalent particles. The thermal conductive model [15] of nanofluid for nanolayer effect is given:

$$k_{\mathrm{nf}}=\frac{k_{\mathrm{pe}}+2k_{\mathrm{f}}+2(k_{\mathrm{pe}}-k_{\mathrm{f}})(1+\beta)^3\phi}{k_{\mathrm{pe}}+2k_{\mathrm{f}}-(k_{\mathrm{pe}}-k_{\mathrm{f}})(1+\beta)^3\phi}k_{\mathrm{f}} \tag{9}$$

where k_{pe} is the thermal conductive of particle defined by:

$$k_{\mathrm{pe}}=\frac{[2(1-\gamma)+(1+\beta)^3(1+2\gamma)]\gamma}{-(1-\gamma)+(1+\beta)^3(1+2\gamma)}k_{\mathrm{s}} \tag{10}$$

Here $\gamma=k_{\mathrm{layer}}/k_{\mathrm{s}}$ is the ratio of nanolayer thermal conductivity to particle thermal conductivity and $\beta=h_{\mathrm{layer}}/R_{\mathrm{p}}$ – the ratio of the nanolayer thickness to the original particle radius. The viscosity model of nanofluid [16] is given:

$$\mu_{\mathrm{nf}}=[1+(2.5\phi_e)+(2.5\phi_e)^2+(2.5\phi_e)^3+\ldots]\mu_{\mathrm{f}} \tag{11}$$

in which $\phi_{\mathrm{e}}=\phi(1+\beta)^3$ and μ_{f} is defined for power law fluid:

$$\mu_{\mathrm{f}}=K\left(\frac{\partial u}{\partial y}\right)^{n-1} \tag{12}$$

By using the following similarity variables:

$$\left.\begin{aligned} \eta = \frac{y}{x}(\mathrm{Re}_x)^{\frac{1}{1+n}},\ \psi = Ux(\mathrm{Re}_x)^{-\frac{1}{1+n}} f(\eta), \\ \theta(\eta) = \frac{T - T_\infty}{T_w - T_\infty},\quad u = \frac{\partial \psi}{\partial y},\ v = -\frac{\partial \psi}{\partial x} \end{aligned}\right\} \tag{13}$$

into eqs. (2)-(5), the non-dimensional ordinary differential equations along with the associated boundary conditions can be written:

$$\frac{\rho_{\mathrm{nf}}}{\rho_{\mathrm{f}}}\left\{f'^2 - \left(\frac{2n}{n+1}\right)ff''\right\} = [1 + (2.5\phi_{\mathrm{e}}) + (2.5\phi_{\mathrm{e}})^2 + ...]\left(n\left|f''\right|^{n-1}\right)f''' + \lambda\frac{(\rho\beta)_{\mathrm{nf}}}{(\rho\beta)_{\mathrm{f}}}\theta \tag{14}$$

$$\mathrm{Pr}\frac{(\rho C_p)_{\mathrm{nf}}}{(\rho C_p)_{\mathrm{f}}}\left\{f'\theta - \left(\frac{2n}{n+1}\right)f\theta'\right\} = \frac{k_{\mathrm{nf}}}{k_{\mathrm{f}}}\theta'' \tag{15}$$

$$\left.\begin{aligned} f(0) = 0,\quad f'(0) = 1,\quad f'(\infty) = 0, \\ \theta(0) = 1,\quad \theta(\infty) = 0 \end{aligned}\right\} \tag{16}$$

where $\mathrm{Pr} = (ax^2/\alpha_{\mathrm{f}})(\mathrm{Re}_x)^{2/(1+n)}$ is the modified Prandtl number, $\lambda = \mathrm{Gr}_x/\mathrm{Re}_x$ – the mixed convection parameter, $\mathrm{Gr}_x = [g\beta(T_w - T_\infty)\rho_\beta x a^{-n}]/K$ – the local Grashof number, and $\mathrm{Re}_x = (\rho_{\mathrm{f}}U^{2-n}x^n)/K$ – the local Reynolds number.

Shear stress and heat flux

The shear stress can be obtained:

$$\tau = K[1 + (2.5\phi_{\mathrm{e}}) + (2.5\phi_{\mathrm{e}})^2 + (2.5\phi_{\mathrm{e}})^3 + ...]\left(\frac{\partial u}{\partial y}\right)^{n-1}\frac{\partial u}{\partial y} \tag{17}$$

The different values for different concentration of polyvinyl alcohol are presented in tab. 1(a) and (b).

Table 1(a). Rheological properties of PVC solutions [17] and power law equation

PVC [%]	Consistency index	Exponent index	Shear stress
2	0.00494	0.790	$\tau = 4.94\cdot10^{-3}[1 + (2.5\phi_{\mathrm{e}}) + (2.5\phi_{\mathrm{e}})^2 + (2.5\phi_{\mathrm{e}})^3 + ...]\left(\frac{\partial u}{\partial y}\right)^{0.790}$
3	0.00925	0.764	$\tau = 9.27\cdot10^{-3}[1 + (2.5\phi_{\mathrm{e}}) + (2.5\phi_{\mathrm{e}})^2 + (2.5\phi_{\mathrm{e}})^3 + ...]\left(\frac{\partial u}{\partial y}\right)^{0.764}$
4	0.01557	0.734	$\tau = 1.56\cdot10^{-2}[1 + (2.5\phi_{\mathrm{e}}) + (2.5\phi_{\mathrm{e}})^2 + (2.5\phi_{\mathrm{e}})^3 + ...]\left(\frac{\partial u}{\partial y}\right)^{0.734}$
5	0.02170	0.718	$\tau = 2.17\cdot10^{-2}[1 + (2.5\phi_{\mathrm{e}}) + (2.5\phi_{\mathrm{e}})^2 + (2.5\phi_{\mathrm{e}})^3 + ...]\left(\frac{\partial u}{\partial y}\right)^{0.718}$

Table 1(b). Thermal conductivity of PVC solutions and heat flux equation

PVC [%]	Thermal conductivity	Heat flux
2	0.586	$q=-0.586\dfrac{k_{\mathrm{pe}}+1.172+2(k_{\mathrm{pe}}-0.586)(1+\beta)^3\phi}{k_{\mathrm{pe}}+1.172-(k_{\mathrm{pe}}-0.586)(1+\beta)^3\phi}\dfrac{\partial T}{\partial y}$
3	0.579	$q=-0.579\dfrac{k_{\mathrm{pe}}+1.158+2(k_{\mathrm{pe}}-0.579)(1+\beta)^3\phi}{k_{\mathrm{pe}}+1.158-(k_{\mathrm{pe}}-0.579)(1+\beta)^3\phi}\dfrac{\partial T}{\partial y}$
4	0. 572	$q=-0.572\dfrac{k_{\mathrm{pe}}+1.44+2(k_{\mathrm{pe}}-0.572)(1+\beta)^3\phi}{k_{\mathrm{pe}}+1.44-(k_{\mathrm{pe}}-0.572)(1+\beta)^3\phi}\dfrac{\partial T}{\partial y}$
5	0.566	$q=-0.566\dfrac{k_{\mathrm{pe}}+1.132+2(k_{\mathrm{pe}}-0.566)(1+\beta)^3\phi}{k_{\mathrm{pe}}+1.132-(k_{\mathrm{pe}}-0.566)(1+\beta)^3\phi}\dfrac{\partial T}{\partial y}$

The wall shear stress in term of skin friction coefficient can be expressed:

$$C_{\mathrm{f}}=\frac{2\tau_w}{\rho u_w^2} \tag{18}$$

where

$$\tau_w=K[1+(2.5\phi_{\mathrm{e}})+(2.5\phi_{\mathrm{e}})^2+(2.5\phi_{\mathrm{e}})^3+\ldots]\left(\frac{\partial u}{\partial y}\right)_{y=0}^{n}$$

and the dimensionless form of skin friction is:

$$C_{\mathrm{f}}\,\mathrm{Re}_x^{1/2}=2[1+(2.5\phi_{\mathrm{e}})+(2.5\phi_{\mathrm{e}})^2+(2.5\phi_{\mathrm{e}})^3+\ldots]f''(0)^n \tag{19}$$

The heat flux is:

$$q=-k_{\mathrm{nf}}\frac{\partial T}{\partial y} \tag{20}$$

The heat transfer coefficient is defined:

$$h=-\frac{k_{\mathrm{nf}}\left(\dfrac{\partial T}{\partial y}\right)_{y=0}}{T_w-T_\infty} \tag{21}$$

The local Nusselt number is given by:

$$\mathrm{Nu}=\frac{hx}{k_{\mathrm{f}}} \tag{22}$$

The dimensionless form of Nusselt number is obtained:

$$\mathrm{Nu}\,\mathrm{Re}_x^{-1/2}=-\frac{k_{\mathrm{nf}}}{k_{\mathrm{f}}}\theta'(0) \tag{23}$$

Solution by optimal homotopy analysis method (OHAM)

We now solve the said non-linear boundary value problem by the OHAM. In order to find explicit formula for $f(\eta)$ and $\theta(\eta)$, first of all, it is obvious that $f(\eta)$ and $\theta(\eta)$ can be expressed by a set of base functions:

$$\{y^k \mathrm{e}^{-ny} \,|\, k \geq 0, \quad n \geq 0\} \tag{24}$$

in the forms:

$$f(\eta) = \sum_{n=0}^{\infty} \sum_{k=0}^{\infty} a_{m,n}^k \eta^k \mathrm{e}^{-n\eta} \tag{25}$$

$$\theta(\eta) = \sum_{n=0}^{\infty} \sum_{k=0}^{\infty} b_{m,n}^k \eta^k \mathrm{e}^{-n\eta} \tag{26}$$

in which $a_{m,n}^k$ and $b_{m,n}^k$ are constant coefficients. Now we choose initial guesses and linear operators of the form:

$$£_1 = \frac{\mathrm{d}^3}{\mathrm{d}\eta^3} - \frac{\mathrm{d}}{\mathrm{d}\eta}, \qquad £_2 = \frac{\mathrm{d}^2}{\mathrm{d}\eta^2} - 1 \tag{27}$$

$$f_0(\eta) = \frac{1}{2} + \left(\frac{1}{2}\mathrm{e}^{-\eta} - 1\right)\mathrm{e}^{-\eta}, \qquad \theta_0(\eta) = \mathrm{e}^{-\eta} \tag{28}$$

and construct the zero-order deformation:

$$(1-p)£_1[\hat{f}(\eta,p) - f_0(\eta)] = pc_0^f N_1[\hat{f}(\eta,p), \hat{\theta}(\eta,p)] \tag{29}$$

$$(1-p)£_2[\hat{\theta}(\eta,p) - \theta_0(\eta,p)] = pc_0^\theta N_2[\hat{f}(\eta,p), \hat{\theta}(\eta,p)] \tag{30}$$

$$\left.\begin{aligned} &\hat{f}(\eta,p) = 0, \quad \frac{\partial \hat{f}(\eta,p)}{\partial \eta} = 1, \quad \hat{\theta}(\eta,p) = 1 \quad \text{at } \eta = 0 \\ &\frac{\partial \hat{f}(\eta,p)}{\partial \eta} = 0, \quad \hat{\theta}(\eta,p) = 0 \quad \text{at } \eta \to \infty \end{aligned}\right\} \tag{31}$$

where $p \in [0,1]$ indicates the embedding parameter and c_0^f and c_0^θ represent auxiliary parameters. Moreover the non-linear operators N_1 and N_2 are defined:

$$\begin{aligned} N_1[\hat{f}(\eta,p), \hat{\theta}(\eta,p)] = &-\frac{\rho_{\mathrm{nf}}}{\rho_{\mathrm{f}}}\left\{m\hat{f}'^2(\eta,p) - \left(\frac{m+1}{2}\right)\hat{f}(\eta,p)\hat{f}''(\eta,p)\right\} + \\ &+[1 + (2.5\phi_{\mathrm{e}}) + (2.5\phi_{\mathrm{e}})^2 + \ldots]\left(n\left|\hat{f}''(\eta,p)\right|^{\varepsilon}\right)\hat{f}'''(\eta,p) + \lambda\frac{(\rho\beta)_{\mathrm{nf}}}{(\rho\beta)_{\mathrm{f}}}\hat{\theta}(\eta,p) \end{aligned} \tag{32}$$

$$N_2[\hat{f}(\eta,p), \hat{\theta}(\eta,p)] = -\mathrm{Pr}\frac{(\rho C_p)_{\mathrm{nf}}}{(\rho C_p)_{\mathrm{f}}}\left\{\hat{f}'\hat{\theta} - \left(\frac{2n}{n+1}\right)\hat{f}\hat{\theta}'\right\} + \frac{k_{\mathrm{nf}}}{k_{\mathrm{f}}}\hat{\theta}'' \tag{33}$$

here $\varepsilon = n - 1$. When $p = 0$, and $p = 1$, we have:

$$\left.\begin{aligned} \hat{f}(\eta,0) = f_0(\eta), \qquad \hat{\theta}(\eta,0) = \theta_0(\eta) \\ \hat{f}(\eta,1) = f(\eta) \qquad \hat{\theta}(\eta,1) = \theta(\eta) \end{aligned}\right\} \tag{34}$$

Expand $\hat{f}(\eta, p)$ and $\hat{\theta}(\eta, p)$ in Taylor's series:

$$\left.\begin{aligned} \hat{f}(\eta, p) = f_0(\eta) + \sum_{m=1}^{\infty} f_m(\eta)\, p^m \\ \hat{\theta}(\eta, p) = \theta_0(\eta) + \sum_{m=1}^{\infty} \theta_m(\eta)\, p^m \end{aligned}\right\} \tag{35}$$

where

$$\theta_m(\eta) = \frac{1}{m!}\frac{\partial \theta^m(\eta, p)}{\partial p^m}\bigg|_{p=0}, \qquad f_m(\eta) = \frac{1}{m!}\frac{\partial f^m(\eta, p)}{\partial p^m}\bigg|_{p=0} \tag{36}$$

The auxiliary parameters are so properly chosen that series converge when $p = 1$ and thus:

$$\left.\begin{aligned} f(\eta) = f_0(\eta) + \sum_{k=1}^{m} f_k(\eta) \\ \theta(\eta) = \theta_0(\eta) + \sum_{k=1}^{m} \theta_k(\eta) \end{aligned}\right\} \tag{37}$$

The m^{th} order deformation problems are:

$$£_1\left[f_m(\eta) - \chi_m f_{m-1}(\eta)\right] = c_0^f R1_m(\eta) \tag{38}$$

$$£_2\left[\theta_m(\eta) - \chi_m \theta_{m-1}(\eta)\right] = c_0^\theta R2_m(\eta) \tag{39}$$

$$\left.\begin{aligned} f_m(0) = 0, \quad \frac{\partial f_m(0)}{\partial \eta} = 1, \quad \theta_m(0) = 0 \\ \frac{\partial f_m(\infty)}{\partial \eta} = 0, \quad \theta_m(\infty) = 0 \end{aligned}\right\} \tag{40}$$

where

$$\begin{aligned} R1_m(\eta) = -\frac{\rho_{\text{nf}}}{\rho_{\text{f}}}\left\{ m \sum_{k=0}^{m} f_k' f_{m-k}' - \left(\frac{m+1}{2}\right)\sum_{k=0}^{m} f_k' f_{m-k}'' \right\} + \\ +[1 + (2.5\phi_{\text{e}}) + (2.5\phi_{\text{e}})^2 + ...]nH_{\varepsilon,k} + \lambda\frac{(\rho\beta)_{\text{nf}}}{(\rho\beta)_{\text{f}}}\theta_m \end{aligned} \tag{41}$$

$$R2_m(\eta) = \Pr\left[n \sum_{k=0}^{m} \theta_k f_{m-k}' - \left(\frac{n+7}{4}\right)\sum_{k=0}^{m} f_k \theta_{m-k}' \right] - \frac{1}{(1-\phi) + \phi\dfrac{(\rho C_p)_{\text{s}}}{(\rho C_p)_{\text{f}}}}\left(\frac{k_{\text{nf}}}{k_{\text{f}}}\theta_m''\right) \tag{42}$$

in which:

$$H_{\varepsilon,k} = \frac{1}{k!}\left\{\frac{\partial^k}{\partial p^k}\left[\frac{\partial^3 \hat{f}}{\partial \eta^3}\left(\frac{\partial^3 \hat{f}}{\partial \eta^3}\right)^{\varepsilon}\right]\right\}\Bigg|_{p=0} \tag{43}$$

$$\chi_m = \begin{cases} 0, & m \le 1 \\ 1, & m > 1 \end{cases} \tag{44}$$

One can note that the series solutions contain the non-zero auxiliary parameters c_0^f and c_0^θ which determine the convergence-region and rate of the homotopy series solutions. To find out the optimal values of c_0^f and c_0^θ, the average residual error are defined by:

$$E_{\mathrm{f}} = \int_0^\infty \left(-\frac{\rho_{\mathrm{nf}}}{\rho_{\mathrm{f}}}\left[mf'^2 - \left(\frac{m+1}{2}\right) ff'' \right] + \right.$$

$$\left. +[1 + (2.5\phi_{\mathrm{e}}) + (2.5\phi_{\mathrm{e}})^2 + \ldots]\left(n\left|f''\right|^{n-1}\right) f''' + \lambda \frac{(\rho\beta)_{\mathrm{nf}}}{(\rho\beta)_{\mathrm{f}}}\theta \right)^2 \mathrm{d}\eta \tag{45}$$

$$E_\theta = \int_0^\infty \left\{ \mathrm{Pr}\frac{(\rho C_p)_{\mathrm{nf}}}{(\rho C_p)_{\mathrm{f}}}\left[f'\theta - \left(\frac{2n}{n+1}\right) f\theta' \right] - \frac{k_{\mathrm{nf}}}{k_{\mathrm{f}}}\theta'' \right\}^2 \mathrm{d}\eta \tag{46}$$

The total squared residual error is follow:

$$E_{\mathrm{total}} = E_{\mathrm{f}} + E_\theta \tag{47}$$

To check the accuracy of OHAM code, the values of $\mathrm{Nu}\,\mathrm{Re}_x^{-1/2}$ presented by Shahzad and Ramzan [18] are compared with obtained results as shown in tab. 2. The optimal values are also shown in tab. 2 and found very good agreement that is infecting a very useful check for the accuracy.

Table 2. Comparison of the obtained results with the ones from the open literature

	n = 1, Pr = 1, M = 1, Nr = 0.5				n = 2, Pr = 1, M = 1, Nr = 0.5			
λ	c_0^f	c_0^θ	Present	Shahzad and Ramzan [18]	c_0^f	c_0^θ	Present	Shahzad and Ramzan [18]
0	–1.15	–0.88	0.6762	0.6762	–0.85	–0.81	0.7232	0.7215
0.5	–1.04	–0.84	0.7170	0.7188	–0.82	–0.80	0.7520	0.7560
1	–0.56	–0.79	0.7532	0.7546	–0.54	–0.77	0.7869	0.7875

Results and discussion

To see effects of emerging parameters involved in the expression of velocity and temperature distributions of shear shear-thinning based nanofluids contained Cu nanoparticles are examined through figs. 2-7. In the study, the value of modified Prandtl number and mixed convection parameter, λ, depend on stretching velocity and fluid nature. To see the effects of particle volume friction, particle size, and different concentration of PVC on velocity and temperature, the values of modified Prandtl number, and λ are given in tab. 3.

Table 3. The values of different parameters corresponding to different nanofluids

U [ms^{-1}]	x [m]	PVC [%]	Pr	Gr_x	Re_x	λ
0.2	0.01	2	8.491	4.1004	764.22	0.00536
–	–	3	14.24	2.3658	442.95	0.00534
–	–	4	20.85	1.5438	289.04	0.00534
–	–	5	27.36	1.1666	218.44	0.00534

In addition, the spherical shape of particle, the nanolayer thickness h_{layer} of 1 nm and nanolayer thermal conductivity k_{layer} of $2k_f$ is used in the proposed model. The effects of particle volume friction on velocity and temperature profiles are displayed in figs. 2 and 3, respectively. Figure 2 points out that when the particle concentration increases then the velocity of fluid reduces. On the other hand, in fig. 3, it is seen that the temperature profile is enhanced by raising the particle volume friction. This is due fact that the temperature of fluid is enlarged when the thermal conductivity is raised. Figures 4 and 5 illustrate the effects of particle radius on the velocity and temperature profiles of nanofluid, respectively. In fig. 4, the velocity of fluid is decreased when size of particle is increased. In addition, it is also observed that temperature of fluid is turn down when radius of particle is enhanced. It is found that when size of particle increases then the Brownian motion of particles slowdown the effects of fluid on velocity and temperature profiles. Figures 6 and 7 demonstrate the behavior of different concentrations of PVC on the velocity and temperature profiles of nanofluid, respectively. It

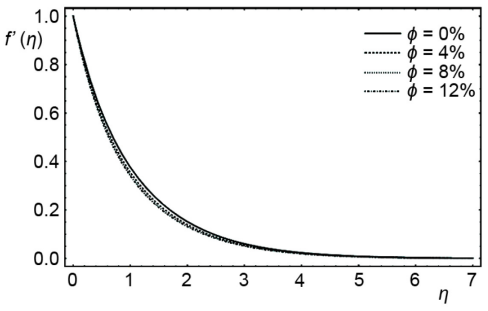

Figure 2. Effect of particle volume friction on velocity profile when R_p = 10 nm

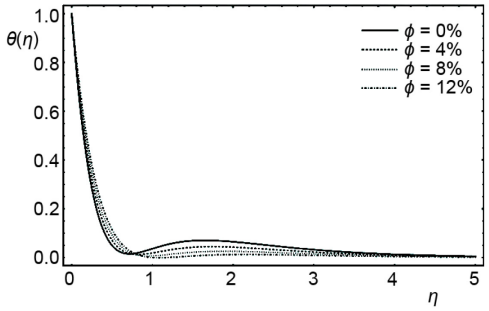

Figure 3. Effect of particle volume friction on temperature profile when R_p = 10 nm

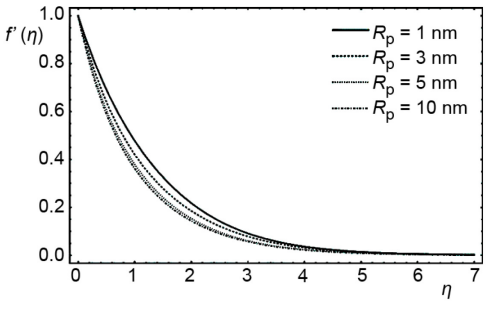

Figure 4. Effect of particle volume friction on velocity profile when ϕ = 4%

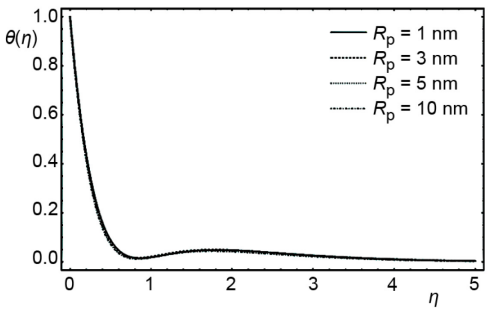

Figure 5. Effect of particle volume friction on temperature profile when ϕ = 4%

is examined in fig. 6, the velocity of nanofluid is increased when concentration of PVC is enhanced. The results in fig. 7 demonstrate that decrement in temperature is occurred near to the wall and far from the wall it is enhanced by increasing the mass concentration in water.

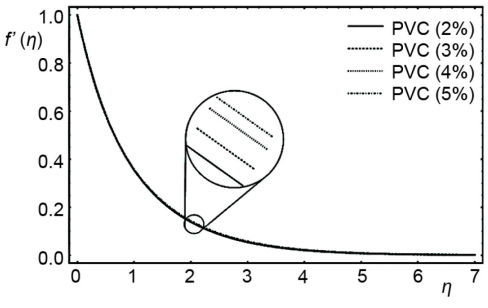

Figure 6. Effect of PVC concentration on velocity profile when ϕ = 4% and R_p = 10 nm

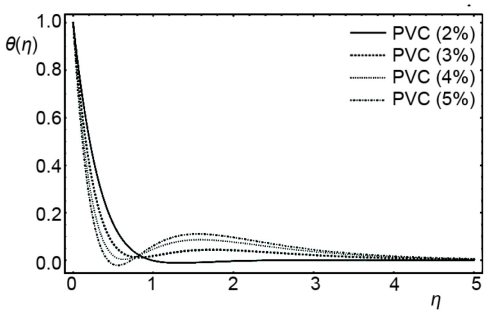

Figure 7. Effect of PVC concentration on temperature profile when ϕ = 4% and R_p = 10 nm

The second set of results show the effects on shear stress and heat flux by adding nanoparticles in PVC solutions. Figures 8 and 9 illustrate the effects of particles volume friction on shear stress in *x*- and *y*-directions, correspondingly. In fig. 8, shear stress increases by increasing the particle volume friction rate. It is observed that shear stress increases near to slit and after some distance no effective change is found. The shear stress in the direction of *y*-axis, increases by increasing the particles volume friction as shown in fig. 9. Figures 10 and 11 show the effects of particle volume friction on heat flux along *x*- and *y*-axis. It is depicted

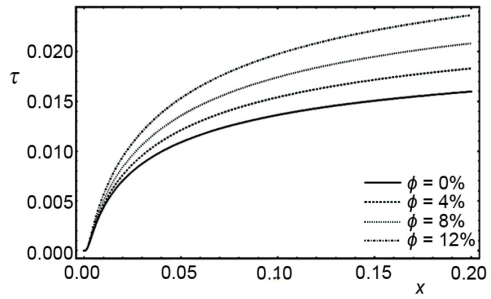

Figure 8. Effect of particle volume friction on shear stress in *x*-direction when R_p = 10 nm

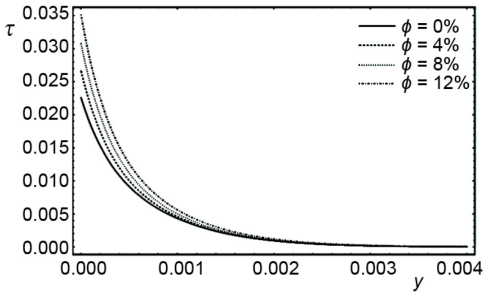

Figure 9. Effect of particle volume friction on shear stress in *y*-direction when R_p = 10 nm

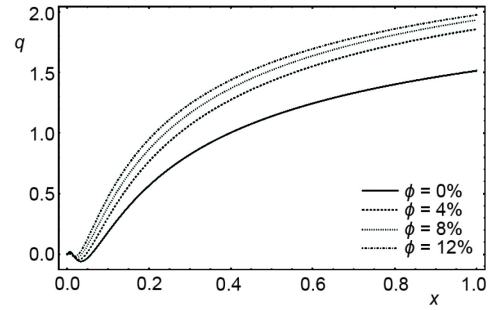

Figure 10. Effect of particle volume friction on heat flux in *x*-direction when R_p = 10 nm

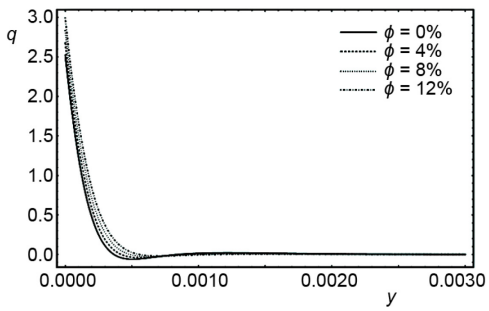

Figure 11. Effect of particle volume friction on heat flux in *y*-direction when R_p = 10 nm

in fig. 10 that heat flux along x-axis increases by increasing the particle volume friction. It is in accordance with the physical expectation that that thermal conductivity increases by enrichment of volume concentration of nanoparticles and as a consequence nanoparticles act the behavior like bridge to pass heat flow. It is also noticed that heat flux near to slit increases readily and then became constant after some length of plate. Figure 11 portrays that when volume friction of nanoparticles increases, the heat flux also increased in the region of boundary layer. Figure 12 shows the effect of volume concentration of particles on thermal resistance at the wall. It is seen that thermal resistance reduces by increasing the concentration of particles. It is happened due to increasing the heat flux enhancement in particle concentration.

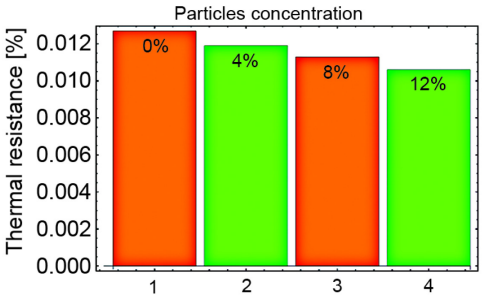

Figure 12. Effect of particle volume friction on thermal resistance when R_p = 10 nm

Conclusions

In this paper, mixed convection heat transfer flow of power law nanofluid over starching plate is investigated. The effects of nanoparticle on velocity, temperature, shear stress, heat flux, and thermal resistance polymer solution with different concentration of PVC are investigated. The main findings of reported results are:

- the velocity of shear thinning fluid declines when particle volume concentration, PVC mass concentration and size of particle are raised,
- the shear stress increases due to increasing the volume concentration,
- the temperature and heat flux of shear thinning fluid enlarged by enhancement of particle volume concentration whereas improvement in temperature with small size of particle is observed, and
- a comparison is also made as a limiting case of presented model.

Nomenclature

C_f – skin friction coefficient, [–]
C_p – effective specific heat capacity, [Jkg^{-1}K^{-1}]
f – dimensionless stream function, [–]
Gr_x – local Grashof number, [–]
h – heat transfer coefficient, [Wm^{-2}K]
K – consistency index, [Pa·s]
k – thermal conductivity, [Wm^{-1}K^{-1}]
Nu – effective Nusselt number, [–]
n – power law index, [–]
Pr – Prandtl number, [–]
q – heat flux, [Wm^{-2}]
Re_x – local Reynolds number, [–]
R_p – radius of nanoparticle, [nm]
T – temperature of fluid, [K]
u – horizontal velocity component, [ms^{-1}]
v – vertical velocity component, [ms^{-1}]
x – horizontal Cartesian co-ordinate, [m]
y – vertical Cartesian co-ordinate, [m]

Greek symbols

α – fluid thermal diffusivity, [m^{2}s^{-1}]
β – thermal expansion coefficient, [K^{-1}]
θ – dimensionless temperature, [–]
λ – mixed convection parameter, [–]
μ – viscosity base fluid, [kgm^{-1}s^{-1}]
ρ – mass density, [kgm^{-3}]

Subscripts

nf – nanofluid
s – solid particle
f – base fluid
layer – nanolayer

References

[1] Baskharone, E. A., *Thermal Science: Essentials of Thermodynamics, Fluid Mechanics and Heat Transfer*, 1st ed., The McGraw-Hill Companies, New York, USA, 2012
[2] Beg, O. A., Magnetohydrodynamic Flows of Nanofluids in Oscillating Tubes with NMR Applications for the Scandinavian Medical Industry, Technical Report, BIO-NANO-2013-5, Gort Engovation, Bradford, UK, 2013
[3] Choi, S. U. S., Eastman J. A., Enhancing Thermal Conductivity of Fluids with Nanoparticles, in: *Proceedings,* International Mechanical Engineering Congress and Exhibition, San Francisco, Cal., USA 1995, pp. 12-17
[4] Shanthi, R., *et al.*, Heat Transfer Enhancement Using Nanofluids – An Overview, *Thermal Science, 16* (2012), 2, pp. 423-444
[5] Han, W. S., *et al.*, Thermal Characteristics of Grooved Heat Pipe with Hybrid Nanofluids, *Thermal Science, 15* (2011), 1, pp. 195-206
[6] Sajadi, A. R., *et al.*, Experimental Study on Turbulent Convective Heat Transfer, Pressure Drop and Thermal Performance of ZnO/Water Nanofluid in a Circular Tube, *Thermal Science, 18* (2014), 2, pp. 1315-1326
[7] Nadeem, S., *et al.*, Numerical Study of MHD Boundary Layer Flow of a Maxwell Fluid past a Stretching Sheet in the Presence of Nanoparticles, *Journal of the Taiwan Institute of Chemical Engineers, 45* (2014), 1, pp. 121-126
[8] Nadeem, S. *et al.*, Nanoparticle Analysis for Non-Orthogonal Stagnation Point Flow of a Third Order Fluid towards a Stretching Surface, *Journal of Computational and* Theoretical Nanoscience*, 10* (2013), 11, pp. 2737-2747
[9] Sheikholeslami, M., *et al.*, Numerical Study of Natural Convection between a Circular Enclosure and a Sinusoidal Cylinder Using Control Volume Based Finite Element Method, *International Journal of Thermal Science, 72* (2013), Oct., pp. 147-158
[10] Sheikholeslami, M., *et al.*, Natural Convection in a Nanofluid Filled Concentric Annulus between an outer Square Cylinder and an Inner Elliptic Cylinder, *Scientia Iranica, Transactions B: Mechanical Engineering, 20* (2013), 4, pp. 1241-1253
[11] Beg, O. A., *et al.*, Comparative Numerical Study of Single-Phase and Two-Phase Models for Bionanofluid Transport Phenomena, *Journal of Mechanics in Medicine and Biology, 14* (2014), 1, DOI: http://dx.doi.org/10.1142/S0219519414500110
[12] Beg, O. A., Lattice Boltzmann Thermal Solvers for Micromorphic and Microstretch Eringen Nanofluids in Spacecraft Propulsion Systems, Technical Report, AERO-NANO-2013-4, Gort Engovation, Bradford, UK, 2013
[13] Liao, S. J., An Optimal Homotopy Analysis Approach for Strongly Non-Linear Differential Equations, *Communications* in *Non-Linear Science and Numerical Simulation*, *15* (2010), 8, pp. 2003-2016
[14] Nadeem, S., *et al.*, Optimized Analytical Solution for Oblique Flow of a Casson-Nanofluid with Convective Boundary Conditions, *International Journal of Thermal Science, 78* (2014), Apr., pp. 90-100
[15] Yu, W., *et al.*, The Role of Interfacial Layers in the Enhanced Thermal Conductivity of Nanofluids: A Renovated Maxwell Model, *Journal of Nanoparticle Research*, *5* (2003), 1-2, pp. 167-171
[16] Avsec, J., Oblak, M., The Calculation of Thermal Conductivity, Viscosity and Thermodynamic Properties for Nanofluids on the Basis of Statistical Nanomechanics, *International Journal of Heat and Mass Transfer, 50* (2007), 21-22, pp. 4331-4341
[17] Etemad, S. G., *et al.*, Theoretical and Experimental Study of the Rheological Behavior of Non-Newtonian Fluids Using Falling Cylinder Rheometer, *Proceedings,* 6th World Congress of Chemical Engineering, Melbourne, Australia, 2011, pp. 23-27
[18] Shahzad, A., Ramzan A., Approximate Analytic Solution for Magneto Hydrodynamic Flow of Non-Newtonian Fluid over a Vertical Stretching Sheet, *Canadian Journal of Applied Sciences, 2* (2012), 3, pp. 202-215

Paper submitted: May 24, 2015
Paper revised: August 28, 2015
Paper accepted: August 28, 2015